



Visible-light-driven selective oxidation of glucose in water with H-ZSM-5 zeolite supported biomimetic photocatalyst

Rui Chen, Changjun Yang*, Quanquan Zhang, Bingguang Zhang, Kejian Deng

Key Laboratory of Catalysis and Materials Science of the State Ethnic Affairs Commission & Ministry of Education, Hubei Province, College of Chemistry and Material Science, South-Central University For Nationalities, Wuhan 430074, China



ARTICLE INFO

Article history:

Received 20 February 2019

Revised 27 April 2019

Accepted 30 April 2019

Keywords:

Glucose

Selective oxidation

H-ZSM-5 zeolite

Iron thioporphyrzine

Photocatalysis

ABSTRACT

A new iron tetra(2,3-bis(butylthio)maleonitrile)porphyrzine ($\text{FePz}(\text{SBU})_8$) has been synthesized, then it was loaded on H-ZSM-5 zeolite to obtain a supported biomimetic photocatalyst H-ZSM-5/ $\text{FePz}(\text{SBU})_8$. Using H_2O_2 as oxidant, the photocatalytic selective oxidation of glucose in water under visible light ($\lambda \geq 420 \text{ nm}$) irradiation was carried out in presence of H-ZSM-5/ $\text{FePz}(\text{SBU})_8$. Under such conditions, the glucose can be efficiently converted into value-added chemicals such as glucaric acid, gluconic acid, arabinose, glycerol and formic acid. More importantly, in comparison with pure $\text{FePz}(\text{SBU})_8$ and pure H-ZSM-5 zeolite, the H-ZSM-5/ $\text{FePz}(\text{SBU})_8$ exhibited a higher photocatalytic activity for glucose oxidation and the formation of glucaric acid was observed only when H-ZSM-5/ $\text{FePz}(\text{SBU})_8$ was used, deriving from the synergistic effect between $\text{FePz}(\text{SBU})_8$ and H-ZSM-5 zeolite. Some reaction parameters of glucose oxidation catalyzed by the H-ZSM-5/ $\text{FePz}(\text{SBU})_8$ were discussed, such as loading amount of $\text{FePz}(\text{SBU})_8$, H_2O_2 :glucose ratio, glucose concentration, and so on. It was demonstrated that the Soret-band of $\text{FePz}(\text{SBU})_8$ contributed more to the visible light photocatalytic activity than the Q-band during the photocatalytic process. The stability of H-ZSM-5/ $\text{FePz}(\text{SBU})_8$ during the photocatalytic process was further evaluated by the reusability test. In addition, the generation of reactive oxygen species was determined by electron spin resonance (ESR) technology and scavenger experiments. A possible reaction pathway of glucose oxidation was also discussed.

© 2019 Elsevier Inc. All rights reserved.

1. Introduction

With the increasing focus on the depletion of petroleum-based resources and environmental pollution, the use of biomass for producing value-added chemicals or other fuels has attracted wide attention because of its characters of renewable, abundance, cheapness and less pollution. Glucose is the most diffuse and cheapest monosaccharide for it can be gained first hand from the hydrolysis of cellulose, the most abundant renewable biomass on Earth [1,2]. The oxidation of glucose can afford a wide variety of value-added chemicals used in the fields of food additive, pharmaceutical and fine chemicals [3,4]. Particularly, glucaric acid produced from the oxidation of both terminal groups is an emerging platform chemical using as a building block chemical. It has been considered as a top value-added chemical from biomass [5]. The traditional oxidation of glucose to value-added chemicals has been extensively investigated using enzymes and heterogeneous catalysts based on metal nanoparticles [6–8]. The application of

photocatalysis in the upgrading of glucose is getting increasing attention. Compared to those energy intensive processes, photocatalytic transformation can be efficiently driven by sunlight and performed at ambient temperature and pressure, such a light driven process seems to be an environmentally friendly, valuable and efficient method for glucose oxidation. Recent advances suggest that partly selective photocatalytic oxidation of glucose to value-added chemicals can be carried out in aqueous media or a mixed solvent of water and acetonitrile using TiO_2 -based catalysts under ultraviolet (UV) light, obtaining a variety of oxidation products including carboxylic acids (glucaric acid, gluconic acid, lactic acid and formic acid) and other oxygenated hydrocarbons (arabinose, erythrose, arabitol, xylitol and glyceraldehyde) [9–14]. It's also worth noting that TiO_2 and Ag/TiO_2 catalysts can also convert glucose to value-added chemicals under visible light because of the formation of a ligand to metal charge transfer complex and the plasmonic effect of Ag, respectively [15,16]. In the light of available energy, UV light only accounts for less than 5% of the total solar energy, while visible light makes up the majority of solar energy [17]. Considering the efficient use of solar energy, it is fundamental that we devise new visible-light-driven photocatalyst that better

* Corresponding author.

E-mail address: yangchangjun@mail.scuec.edu.cn (C. Yang).

utilize solar energy and still exhibit high activity and selectivity for organic synthetic reaction.

Metallothioporphyrazines (MPzs) possessing sulfur-containing groups in macrocyclic periphery are a type of macrocyclic compound which have an extensive system of delocalized π electrons. They have attracted an increasing interest in recent years due to their peculiar photophysical, photochemical and electrochemical properties [18–20]. Specifically, MPzs are considered as biomimetic photocatalysts because of their strong absorption in the visible region, which can nicely meet the purpose of using sunlight. In our previous research, it has been reported that MPzs exhibited a unique photocatalytic activity for activating hydrogen peroxide or dioxygen under visible light, which are applied to the selective organic transformations under mild conditions. For example, using cobalt thioporphyrazine as photocatalyst, the benzyl alcohol and amine could be highly selectively oxidized to benzoic acid and imine under visible light irradiation, respectively [21,22]. The easy excitation by visible light and the ability of participating in various photophysico-chemical processes make MPzs as promising candidates for excellent photocatalysts.

The molecular structure of MPz can be modified by modulating the peripheral substitutes, changing the central metal or expanding the π -electron system [23,24]. Herein, a new iron tetra(2,3-bis(butylthio)maleonitrile)porphyrazine ($\text{FePz}(\text{SBU})_8$) was synthesized, the molecular structure of $\text{FePz}(\text{SBU})_8$ was shown in Fig. 1. Then the $\text{FePz}(\text{SBU})_8$ complex was loaded onto the H-ZSM-5 zeolite which has large specific surface area and high chemical stability, obtaining the photocatalyst H-ZSM-5/ $\text{FePz}(\text{SBU})_8$. Using H_2O_2 as oxidant, the photocatalytic oxidation of glucose under visible light ($\lambda \geq 420$ nm) irradiation was carried out by using H-ZSM-5/ $\text{FePz}(\text{SBU})_8$ photocatalysts in water. It turned out that $\text{FePz}(\text{SBU})_8$ was an efficient biomimetic photocatalyst for oxidation of glucose to value-added chemicals, such as glucaric acid, gluconic acid, arabinose, glycerol and formic acid. Moreover, the active oxygen species generated in the photocatalytic process were identified and the possible reaction pathway of glucose oxidation was also discussed.

2. Experimental

2.1. Materials and instruments

All chemicals and solvents used in this work were purchased from Aladdin Chemicals Co., Ltd and Sinopharm Chemical Reagent Co., Ltd, and all of them were used as received without further purification.

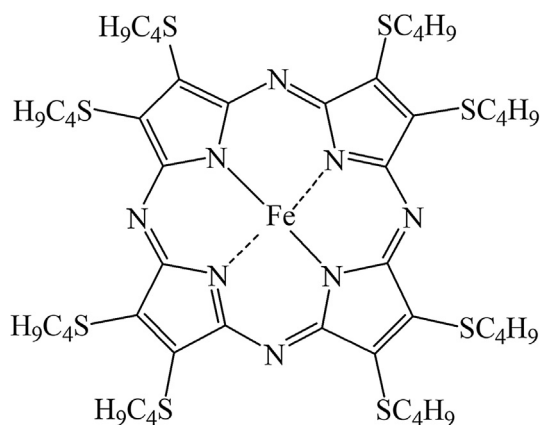


Fig. 1. Molecular structure of iron tetra(2,3-bis(butylthio)maleonitrile)porphyrazine ($\text{FePz}(\text{SBU})_8$).

High-resolution mass spectra were obtained on an AB/5800 MALDI-TOF mass spectrometer. The ultraviolet-visible (UV-vis) spectra of catalyst in solution were measured by a Shimadzu UV-2600 UV-vis spectrophotometer, and the UV-vis diffuse reflectance spectra (DRS) of supported catalysts were also acquired by the Shimadzu UV-2600 UV-vis spectrophotometer equipped with an integrating sphere attachment, using BaSO_4 as the reference material. ^1H NMR spectra were recorded with a Bruker Avance III 400 spectrometer. The morphology of the catalyst was characterized by scanning electron microscope (SEM) (SU8010, HITACHI) and transmission electron microscopy (TEM) (Tecni G20, USA). The X-ray photoelectron spectra (XPS) analysis of the catalysts was recorded on a VG Multilab-2000 spectrometer (Thermo Electron Corporation) with a monochromatic Mg $K\alpha$ source and a charge neutralizer. The X-ray diffraction (XRD) patterns were conducted using a D8-advance powder diffractometer (German Bruker). The reactive oxygen species were determined by electron spin resonance (ESR) spectra, which were performed by a JES-FA200 spectrometer. The photocurrents were measured with a CHI 760E electrochemical workstation.

2.2. Synthesis of iron tetra(2,3-bis(butylthio)maleonitrile)porphyrazine

The metal-free tetra(2,3-bis(butylthio)maleonitrile)porphyrazine ($\text{H}_2\text{Pz}(\text{SBU})_8$) was synthesized in the following procedure. Magnesium butoxide solution was firstly prepared by the reaction of magnesium tablet (0.06 g) with butanol (100 mL) at reflux temperature for 48 h. Then the precursor 2,3-bis(butylthio)maleonitrile (3 g) was added into the preceding magnesium butoxide solution, a dark-green solution was obtained after reaction for 24 h at reflux temperature under stirring condition. Removal of the solvent by reduced pressure distillation gave a crude solid formed. The obtained products were subsequently dissolved in trifluoroacetic acid (5 mL), and the mixture was stirred for additional 8 h in dark in order to remove the center metal magnesium. After that, the solution was plunged into purified water to deposit the target product metal-free $\text{H}_2\text{Pz}(\text{SBU})_8$, the dark purple products were obtained by filtration, which were thoroughly washed with ammonia solution, water and methanol. The target products formed was further purified on silica gel chromatography column using dichloromethane (CH_2Cl_2)/petroleum ether (PE) (1:1, v/v) as an eluent. The target product $\text{H}_2\text{Pz}(\text{SBU})_8$ was characterized with UV-vis spectrum and ^1H NMR spectrum, the characteristic structure datas for the product were shown as following: 2.18 g (yield 69%); UV-vis λ_{max} (in CH_2Cl_2): Q-band: 712 nm and 640 nm; Soret-band: 507 nm, B-band: 350 nm, see Fig. 2(A); ^1H NMR (400 MHz, CDCl_3): δ = 4.1 (t, 2H, $-\text{SCH}_2-$), 1.9 (m, 2H, $-\text{CH}_2-$), 1.6 (m, 2H, $-\text{CH}_2-$), 0.9 (t, 3H, $-\text{CH}_3$), -1.1 (t, 2H, $-\text{NH}-$), see Fig. 2(B).

Metal-free $\text{H}_2\text{Pz}(\text{SBU})_8$ (0.308 g) and iron acetylacetonate (0.312 g) were respectively added into pyridine (50 mL), then the mixture was continuously stirred for 10 h at 115 $^\circ\text{C}$, the color of the solution changed from purple to green during the reaction. After the reaction was completed, the target product $\text{FePz}(\text{SBU})_8$ was obtained by removing the solvent pyridine using reduced pressure distillation, which was further purified on silica gel chromatography column using CH_2Cl_2 /methanol (9:1, v/v) as an eluent. The target product $\text{FePz}(\text{SBU})_8$ was characterized with UV-vis spectrum and MALDI-TOF MS, the characteristic structure datas for the product were shown as following: 0.234 g (yield 72%); UV-vis λ_{max} (in CH_2Cl_2): Q-band: 644 nm; Soret-band: 501 nm, B-band: 366 nm, see Fig. 3(A); MALDI-TOF MS: m/z = 1073.3 $[\text{M}+\text{H}]^+$, see Fig. 3(B).

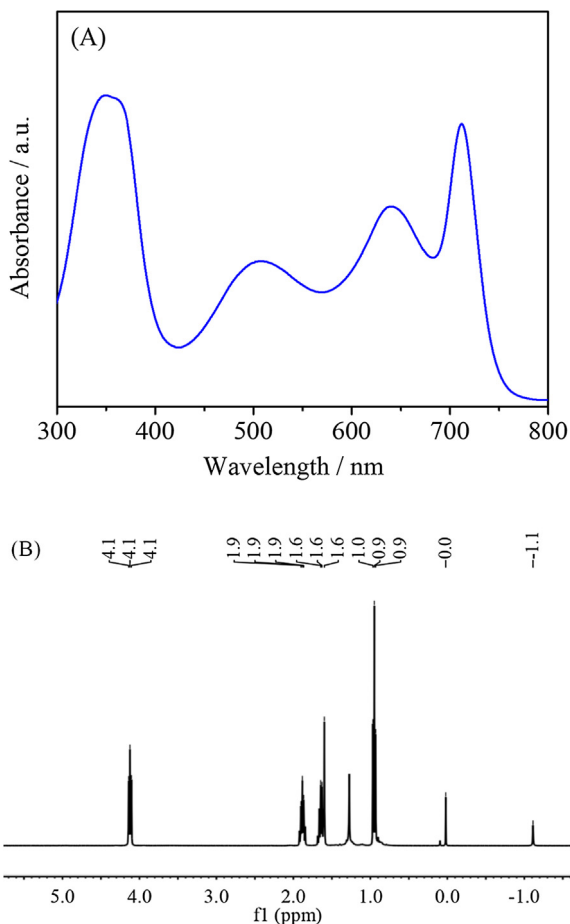


Fig. 2. UV-vis spectrum of metal-free $\text{H}_2\text{Pz}(\text{SBu})_8$ in CH_2Cl_2 (A) and the ^1H NMR spectrum of $\text{H}_2\text{Pz}(\text{SBu})_8$ in CDCl_3 (B).

2.3. Preparation of H-ZSM-5/FePz(SBu)₈

ZSM-5 zeolite was synthesized in the light of the reported literature [25]. To obtain H-type ZSM-5 (H-ZSM-5) zeolite, the prepared ZSM-5 zeolite was added into 1 L 1 mol L^{-1} NH_4NO_3 aqueous solution, which was further stirred at room temperature for 24 h. The target product H-ZSM-5 zeolite was obtained by filtration and washed thoroughly with ethanol and water, which was then dried at $120 \text{ }^\circ\text{C}$ for 12 h and finally calcined at $550 \text{ }^\circ\text{C}$ for 4 h, obtaining H-ZSM-5 zeolite.

In a typical preparation procedure on H-ZSM-5/FePz(SBu)₈, 30 mg FePz(SBu)₈ was firstly dissolved in 30 mL CH_2Cl_2 by means of ultrasonication. Then 1 g H-ZSM-5 zeolite was added into the above solution under the action of magnetic stirring, the mixture was stirred continuously for 5 h. After that, the supported photocatalyst H-ZSM-5/FePz(SBu)₈ was obtained by removing the solvent CH_2Cl_2 using reduced pressure distillation, the content of FePz(SBu)₈ supported on the H-ZSM-5 zeolite was equal to 3%. A range of H-ZSM-5/FePz(SBu)₈ photocatalysts with different content of FePz(SBu)₈, such as 1%, 5% and 7%, were also prepared on the grounds of the same experimental process.

2.4. Photocatalytic oxidation of glucose

In a typical photocatalytic reaction, 30 mg H-ZSM-5/FePz(SBu)₈ photocatalysts were firstly dispersed into 30 mL 3 mmol L^{-1} aqueous glucose solution in a Pyrex vessel with a circling water-cooled jacket by ultrasonication for 5 min. Then an additional H_2O_2 with a

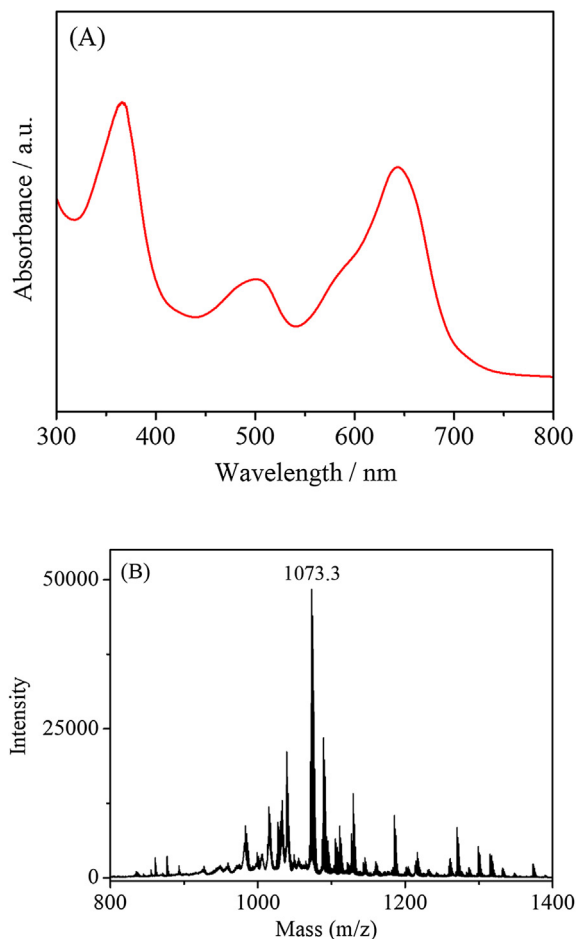


Fig. 3. UV-vis spectrum of FePz(SBu)₈ in CH_2Cl_2 (A) and the MALDI-TOF MS of FePz(SBu)₈ (B).

H_2O_2 :glucose ratio of 3.3:1 was added into the above suspension and continually stirred for 10 min. After that, the reaction mixture was irradiated by a Xe lamp (Beijing China Education Au-light Co., Ltd) with a 420 nm cutoff filter. In order to control the photocatalytic reaction at ambient temperature, the cooling water was circulated through the circling water-cooled jacket located around the reactor. Sample solutions were taken at specific times and then immediately filtered by $0.22 \text{ } \mu\text{m}$ membranes before analyses.

The glucose conversion and the selectivity of oxidation product were monitored using a Dionex UltiMate 3000 HPLC system equipped with a refractive index (RI) (ERC RefractoMax520) detector, a Shodex SUGAR SH-1011 column ($8 \text{ mm} \times 300 \text{ mm}$) and an aqueous 0.4 mmol L^{-1} H_2SO_4 solution as an eluent with a flow rate of 0.6 mL min^{-1} were used. The products generated during the reaction were identified by comparison with standard samples and further confirmed by high performance liquid chromatography-mass (HPLC-MS). HPLC-MS analysis was performed on a Shimadzu LCMS-8050 triple quadrupole mass spectrometer with C18 column ($4.6 \text{ mm} \times 250 \text{ mm}$).

The conversion of glucose and selectivity of oxidation products were calculated using the following formulas.

$$\text{Conversion} = \frac{[\text{glucose}]_i - [\text{glucose}]_t}{[\text{glucose}]_i} \times 100\%$$

$$\text{Selectivity} = \frac{[\text{product}]_t}{[\text{glucose}]_i - [\text{glucose}]_t} \times 100\%$$

In the above formulas, $[\text{glucose}]_i$ stands for the initial molar concentration of substrate glucose. $[\text{glucose}]_t$ and $[\text{product}]_t$ represent the

molar concentration of substrate glucose and a product after t time of reaction, respectively.

3. Results and discussion

3.1. Characterization of metal-free thioporphyrazine and iron thioporphyrazine

The UV–vis absorption spectrum of metal-free $\text{H}_2\text{Pz}(\text{SBU})_8$ in CH_2Cl_2 was shown in Fig. 2(A). It could be seen that three types of characteristic bands, such as Q-band at 712 nm and 640 nm, Soret-band at 507 nm and B-band at 350 nm, presented in the spectra of $\text{H}_2\text{Pz}(\text{SBU})_8$. Specifically, the splitting two peaks of Q-band is an important feature of free-base porphyrazine. Moreover, the ^1H NMR spectrum of $\text{H}_2\text{Pz}(\text{SBU})_8$ in CDCl_3 was shown in Fig. 2 (B). It shows four kinds of hydrogens, namely, 4.1 (t, 2H, $-\text{SCH}_2-$), 1.9 (m, 2H, $-\text{CH}_2-$), 1.6 (m, 2H, $-\text{CH}_2-$) and 0.9 (t, 3H, $-\text{CH}_3$) in the peripheral butylthio group, and the inner hydrogen -1.1 (t, 2H, $-\text{NH}-$) of macrocycle. The result of ^1H NMR further verifies the synthesis of metal-free $\text{H}_2\text{Pz}(\text{SBU})_8$.

The as-prepared metal-free $\text{H}_2\text{Pz}(\text{SBU})_8$ directly reacted with iron acetylacetonate in pyridine solution to generate the target product $\text{FePz}(\text{SBU})_8$ with a yield of 72%. The UV–vis absorption spectrum of $\text{FePz}(\text{SBU})_8$ in CH_2Cl_2 was presented in Fig. 3(A). It is obvious that the splitted Q-band disappeared in the spectrum of $\text{FePz}(\text{SBU})_8$ in comparison to that of metal-free $\text{H}_2\text{Pz}(\text{SBU})_8$, indicating that the coordination reaction of iron ion had successfully occurred under current conditions. Meanwhile, the MALDI-TOF MS of $\text{FePz}(\text{SBU})_8$ has $m/z = 1073.3$ $[\text{M}+\text{H}]^+$ as shown in Fig. 3(B), which is in good consistent with the molecular weight of $\text{FePz}(\text{SBU})_8$. From the XPS analysis as shown in Fig. S1, it could be observed that the presence of the Fe(II) peaks at 720.95 eV and 708.20 eV, which correspond to the binding energies of $\text{Fe}2\text{p}_{1/2}$ and $\text{Fe}2\text{p}_{3/2}$ [26].

3.2. Characterization of H-ZSM-5/ $\text{FePz}(\text{SBU})_8$

Fig. 4 shows that the X-ray diffraction (XRD) patterns of pure H-ZSM-5 zeolite and H-ZSM-5/ $\text{FePz}(\text{SBU})_8$ samples. As can be seen in Fig. 4a, the prepared H-ZSM-5 zeolite sample shows Bragg diffraction peaks with 2θ at 7.98° , 8.78° , 23.09° , 23.88° and 24.41° , indicating that the sample consists of highly crystalline MFI phase [25,27]. The morphology of the prepared H-ZSM-5 zeolite sample was also observed by TEM and SEM, which were shown in

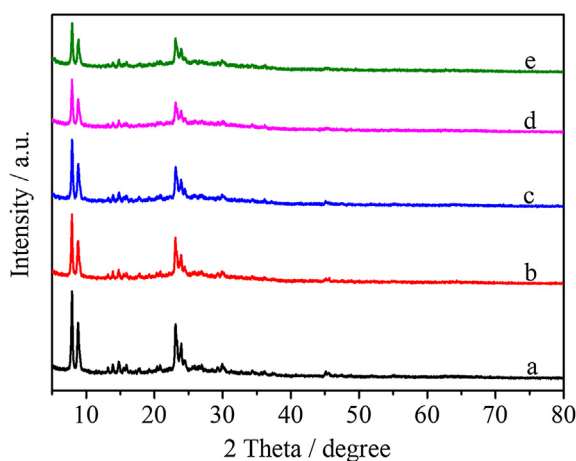


Fig. 4. X-ray diffraction (XRD) patterns of pure H-ZSM-5 zeolite and H-ZSM-5/ $\text{FePz}(\text{SBU})_8$. (a) pure H-ZSM-5 zeolite; (b) H-ZSM-5/ $\text{FePz}(\text{SBU})_8$ (1%); (c) H-ZSM-5/ $\text{FePz}(\text{SBU})_8$ (3%); (d) H-ZSM-5/ $\text{FePz}(\text{SBU})_8$ (5%); (e) H-ZSM-5/ $\text{FePz}(\text{SBU})_8$ (7%).

Figs. S2 and 5(A), respectively. From Figs. S2 and 5(A), it is displayed that the prepared H-ZSM-5 zeolite nanoparticles are spherical in shape. After a small quantity of $\text{FePz}(\text{SBU})_8$ complex were supported on the H-ZSM-5 zeolite, such as 1%, 3%, 5% and 7%, the peak positions of H-ZSM-5 zeolite did not change in the XRD patterns of H-ZSM-5/ $\text{FePz}(\text{SBU})_8$, indicating that the loading process of $\text{FePz}(\text{SBU})_8$ has little effect on the bulk structure of H-ZSM-5 zeolite.

The SEM image of H-ZSM-5/ $\text{FePz}(\text{SBU})_8$ (5%) was shown in Fig. 5 (B). Compared with the morphology of bare H-ZSM-5 zeolite (Fig. 5 (A)), it could be seen that the shape of the H-ZSM-5 zeolite remained essentially unchanged before and after loading with $\text{FePz}(\text{SBU})_8$, which is in good agreement with the above XRD analysis. However, a net structure of film-like layer (see yellow ring in Fig. 5(B)) was clearly presented on the surface of H-ZSM-5 zeolite for H-ZSM-5/ $\text{FePz}(\text{SBU})_8$ sample, which should be the deposited $\text{FePz}(\text{SBU})_8$, that is to say, $\text{FePz}(\text{SBU})_8$ is distributed on the surface of H-ZSM-5 zeolite. This result indicated that the $\text{FePz}(\text{SBU})_8$ was successfully loaded on the H-ZSM-5 zeolite.

UV–vis DRS was carried out to analyze the optical spectral response of pure H-ZSM-5 zeolite and H-ZSM-5/ $\text{FePz}(\text{SBU})_8$, as shown in Fig. 6. From Fig. 6, it was observed that the support H-ZSM-5 zeolite showed poor absorption from 300 nm to 800 nm. But for H-ZSM-5/ $\text{FePz}(\text{SBU})_8$ samples, all samples display the feature peaks of $\text{FePz}(\text{SBU})_8$ molecule such as Q-band and B-band, this provides further evidence that $\text{FePz}(\text{SBU})_8$ successfully loaded onto the surface of H-ZSM-5 zeolite, which is also consistent with the SEM observation. Meanwhile, the UV–vis DRS datas provide additional important information that H-ZSM-5/ $\text{FePz}(\text{SBU})_8$ samples have intensive absorption in the visible light region, implying that they can be served as visible light photocatalysts to drive the photocatalytic reactions.

3.3. Photocatalytic performance

The photocatalytic performance of H-ZSM-5/ $\text{FePz}(\text{SBU})_8$ photocatalyst for oxidation of glucose in water was carried out under visible light ($\lambda \geq 420$ nm) irradiation. Table 1 shows the results of exploratory experiments of the glucose oxidation under different conditions, obtaining insight into the excellent performance of the H-ZSM-5/ $\text{FePz}(\text{SBU})_8$ catalyst for oxidation of glucose to value-added chemicals. In absence of any catalyst, the conversion of glucose is only 2.2% in presence of H_2O_2 under visible light irradiation and the oxidation product is arabinose (Table 1, Entry 1). As it is seen, 4.9% glucose conversion is obtained in presence of pure $\text{FePz}(\text{SBU})_8$, the oxidation products are gluconic acid, arabinose, glycerol and formic acid, under such conditions, the mass of $\text{FePz}(\text{SBU})_8$ catalyst is equal to that in the H-ZSM-5/ $\text{FePz}(\text{SBU})_8$ (5%) composite in order to compare the photocatalytic activity (Table 1, Entry 2). The reaction of glucose oxidation could also occur in presence of H-ZSM-5 zeolite with 1.9% conversion, producing a very small quantity of gluconic acid and arabinose (Table 1, Entry 3). It is known that $\text{Fe}^{3+}/\text{H}_2\text{O}_2$ system is the famous Fenton reagent, therefore, the glucose conversion in presence of FeCl_3 is also conducted under visible light irradiation. Although 99.1% glucose conversion is achieved on FeCl_3 catalyst, only formic acid with a selectivity of 6.8% is obtained (Table 1, Entry 4). Compared with the above several system, H-ZSM-5/ $\text{FePz}(\text{SBU})_8$ displays the excellent performance of oxidation of glucose to value-added chemicals, five value-added products such as glucaric acid, gluconic acid, arabinose, glycerol and formic acid are obtained, the total selectivity for five products is 79.8% of 35.8% glucose conversion (Table 1, Entry 5). The total selectivity is less than 100%, maybe because the glucose is mineralized to CO_2 and H_2O . The most interesting finding is that glucaric acid is obtained with a selectivity of 13.1% in the H-ZSM-5/ $\text{FePz}(\text{SBU})_8$ photocatalytic system, while

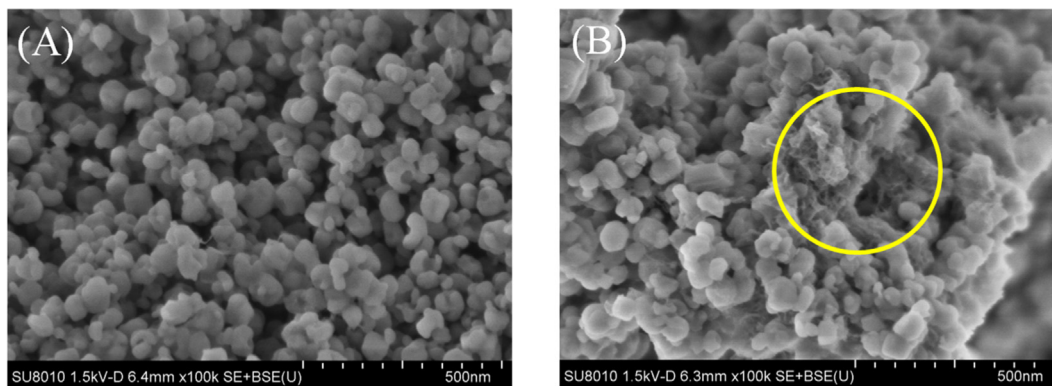


Fig. 5. SEM images of pure H-ZSM-5 zeolite (A) and H-ZSM-5/FePz(SBu)₈ (5%) (B).

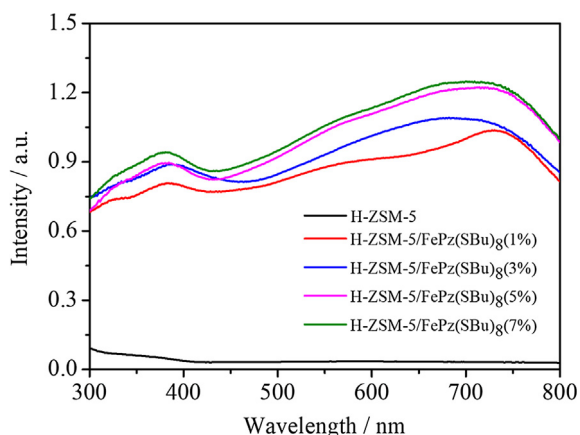


Fig. 6. UV-vis diffuse reflectance spectra (DRS) of pure H-ZSM-5 zeolite and H-ZSM-5/FePz(SBu)₈.

no glucaric acid is formed under the conditions of pure FePz(SBu)₈ or pure H-ZSM-5 zeolite. These results indicate that there exists a synergistic effect between FePz(SBu)₈ and H-ZSM-5 zeolite, which is beneficial to the oxidation of glucose and the formation of glucaric acid. In contrast, almost no conversion of glucose occurred in the dark over the H-ZSM-5/FePz(SBu)₈ catalyst (Table 1, Entry 6). Meanwhile, increasing the light intensity results in enhance-

ment of the conversion rate of glucose (Fig. S3), indicating that the photocatalytic activity of the H-ZSM-5/FePz(SBu)₈ depends on the intensity of incident light. These results clearly display that the glucose oxidation is undoubtedly driven by visible light. When O₂ is inlet, the glucose conversion over the H-ZSM-5/FePz(SBu)₈ is only about 1.5% (Table 1, Entry 7).

Photocatalytic oxidation of glucose in water in presence of Na-ZSM-5/FePz(SBu)₈ or SiO₂/FePz(SBu)₈ were also performed under the same reaction conditions, it was found that the photocatalytic activities of both catalysts were lower than that of H-ZSM-5/FePz(SBu)₈ and no glucaric acid was formed in both catalytic systems (Table 1, entries 8 and 9), indicating that H-ZSM-5 zeolite is a better support for FePz(SBu)₈ for glucose oxidation in water. In addition, the photocatalytic oxidation of glucose were conducted under irradiation of $\lambda = 500$ nm visible light and $\lambda = 650$ nm visible light in presence of H-ZSM-5/FePz(SBu)₈. It could be seen that the glucose conversion obtained with $\lambda = 500$ nm visible light is higher than that obtained with $\lambda = 650$ nm visible light (Table 1, entries 10 and 11). Therefore, it was proposed that the Soret-band of FePz(SBu)₈ contributed more to the visible light photocatalytic activity than the Q-band during the photocatalytic process.

The effect of loading amounts of FePz(SBu)₈ on the photocatalytic oxidation of glucose to value-added chemicals was further examined, as shown in Fig. 7. Inspection of Fig. 7 suggests that the glucose conversion improved with increasing the loading amounts, which changes from 6.4% to 46% in the loading range

Table 1
The photocatalytic oxidation of aqueous glucose under different conditions.^a

Entry	Catalyst	Conversion/%	Selectivity/%					Σ Selectivity/%
			GAA	GOA	Ab	Gly	FA	
1	without	2.2	–	–	87.1	–	–	87.1
2 ^b	FePz(SBu) ₈	4.9	–	27.5	31.8	10.6	7.8	77.8
3	H-ZSM-5	1.9	–	35.7	54.3	–	–	90.0
4	FeCl ₃	99.1	–	–	–	–	6.8	6.8
5	H-ZSM-5/FePz(SBu) ₈ (5%)	35.8	13.1	31.9	17.3	1.7	13.0	79.8
6 ^c	H-ZSM-5/FePz(SBu) ₈ (5%)	–	–	–	–	–	–	–
7 ^d	H-ZSM-5/FePz(SBu) ₈ (5%)	1.5	–	17.4	80.5	–	–	97.9
8	Na-ZSM-5/FePz(SBu) ₈ (5%)	21.7	–	34.1	12.8	8.4	10.3	65.7
9	SiO ₂ /FePz(SBu) ₈ (5%)	6.0	–	21.8	25.3	8.4	6.2	61.7
10 ^e	H-ZSM-5/FePz(SBu) ₈ (5%)	14.3	11.1	24.6	22.2	7.3	20.2	85.4
11 ^f	H-ZSM-5/FePz(SBu) ₈ (5%)	7.9	21.9	33.1	12.4	6.8	16.0	90.1

^a Reaction conditions: catalyst (30 mg), aqueous glucose (3 mmol L⁻¹, 30 mL), H₂O₂ with a H₂O₂:glucose ratio of 3.3:1, $\lambda \geq 420$ nm visible light (light intensity: 1.70 W cm⁻²), reaction for 4 h.

^b FePz(SBu)₈ (1.5 mg).

^c Without visible light irradiation.

^d Without adding H₂O₂.

^e $\lambda = 500$ nm visible light (light intensity: 1.70 W cm⁻²).

^f $\lambda = 650$ nm visible light (light intensity: 1.70 W cm⁻²). (Note: GAA-glucaric acid, GOA-gluconic acid, Ab-arabinose, Gly-glycerol, FA-formic acid.).

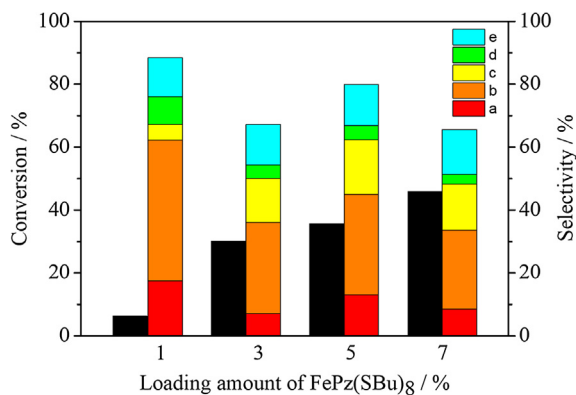


Fig. 7. Effect of loading amounts of FePz(SBu)₈ on the photocatalytic oxidation of glucose under visible light irradiation. Reaction conditions: catalyst (30 mg), aqueous glucose (3 mmol L⁻¹, 30 mL), H₂O₂ with a H₂O₂:glucose ratio of 3.3:1, λ ≥ 420 nm visible light (light intensity: 1.70 W cm⁻²), reaction for 4 h. a: glucaric acid; b: gluconic acid; c: arabinose; d: glycerol; e: formic acid. (Note: black bar and color bar represent the glucose conversion and product selectivity, respectively.)

from 1% to 7%. It indicates that the loading amount of FePz(SBu)₈ has a positive effect on the photocatalytic activity of H-ZSM-5/FePz(SBu)₈. Different loading amounts of FePz(SBu)₈ have a limited impact on the total selectivity of oxidation products. In all cases, the gluconic acid is the main oxidation product, which has a maximum selectivity with 44.7% when the loading is 1%. While by increasing the loading amount there exists a downward trend for the selectivity of glucaric acid. The arabinose exhibits a high selectivity when the loading amount of FePz(SBu)₈ exceeds 1%. Considering the substrate conversion and product selectivity, it appears that the best loading of FePz(SBu)₈ for glucose oxidation under the experimental conditions used in this study is 5%.

3.4. Effect of reaction conditions for glucose oxidation

The effect of H₂O₂:glucose ratio on the photocatalytic oxidation of glucose to value-added chemicals was examined in presence of H-ZSM-5/FePz(SBu)₈(5%). As illustrated in Fig. 8, it could be seen that the conversion of glucose increases from 19.1% to 86.3% with a variation of H₂O₂:glucose ratio from 2.2:1 to 4.4:1. However, the total selectivity of oxidation products shows a downward trend with the increase of H₂O₂:glucose ratio. When H₂O₂:glucose ratio is low, such as 2.2:1, the total selectivity for oxidation products

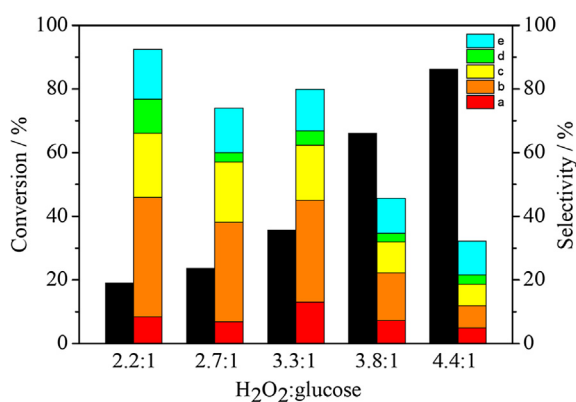


Fig. 8. Effect of H₂O₂:glucose ratio on the photocatalytic oxidation of glucose in presence of H-ZSM-5/FePz(SBu)₈(5%). Reaction conditions: catalyst (30 mg), aqueous glucose (3 mmol L⁻¹, 30 mL), λ ≥ 420 nm visible light (light intensity: 1.70 W cm⁻²), reaction for 4 h. a: glucaric acid; b: gluconic acid; c: arabinose; d: glycerol; e: formic acid. (Note: black bar and color bar represent the glucose conversion and product selectivity, respectively.)

could be reached up to 92.4%, while the total selectivity for glucaric acid and gluconic acid is up to 45.9%. Meanwhile, a different evolution trend for selectivity of each product is also observed. For example, a maximum selectivity of glucaric acid is acquired when H₂O₂:glucose ratio is 3.3:1, and then a gradual reduction of the selectivity is detected when H₂O₂:glucose ratio increases from 3.3:1 to 4.4:1. The selectivity in gluconic acid shows the highest value of 37.5% in a low H₂O₂:glucose ratio, such as 2.2:1, a further increase in H₂O₂:glucose ratio gradually decreases the selectivity of gluconic acid, a similar trend to three other compounds is also observed.

Subsequently, the effect of glucose concentration on the photocatalytic oxidation of glucose to value-added chemicals was further investigated in the range from 1 mmol L⁻¹ to 10 mmol L⁻¹, as showed in Fig. S4. At a low concentration of 1 mmol L⁻¹, the conversion of glucose could reach up to 88.7% after reaction for 4 h, but the total selectivity of oxidation products is only about 13.8%, maybe because the generated products suffer from the attack of active oxygen species to cause the deep oxidation in a low substrate concentration. With increasing the glucose concentration, the total selectivity of oxidation products exhibits a significant improvement, for the probability that active oxygen species attack the substrate is markedly increased in a high substrate concentration. It is noteworthy that the total selectivity for glucaric acid and gluconic acid reaches up to 45% when glucose concentration is 3 mmol L⁻¹. While when the substrate concentration exceeds 3 mmol L⁻¹, no remarkable change of the glucose conversion is observed, it is probably because of the limited amount of oxidant.

3.5. Reusability of the photocatalyst

The recyclability of catalyst plays a significant role in its industrial application. For this purpose, the repeatability of H-ZSM-5/FePz(SBu)₈ photocatalyst in the photocatalytic conversion of glucose was examined. As shown in Fig. 9, it can be seen that about 40.6% of glucose is converted at the first run, the conversion of glucose is decreased to 25% after five consecutive runs. The slight reduction of photocatalytic activity maybe result from the fall out of FePz(SBu)₈ from the surface of H-ZSM-5 during the reaction process. With respect to the selectivity of oxidation products, no remarkable change is observed. It suggests that the H-ZSM-5/FePz(SBu)₈ material as a photocatalyst are basically stable in the reaction of glucose oxidation.

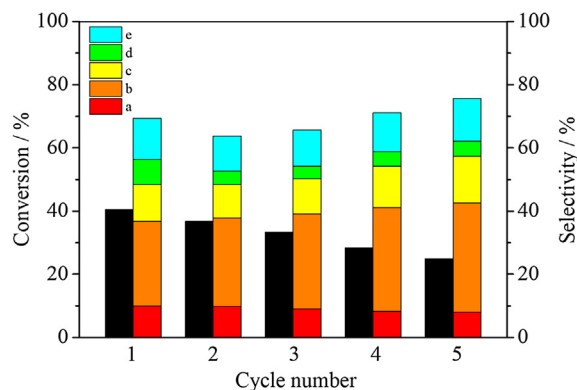


Fig. 9. Reusability of H-ZSM-5/FePz(SBu)₈(5%) for photocatalytic oxidation of glucose in water under visible light irradiation. Reaction conditions: catalyst (30 mg), aqueous glucose (3 mmol L⁻¹, 30 mL), H₂O₂ with a H₂O₂:glucose ratio of 3.3:1, λ ≥ 420 nm visible light (light intensity: 1.70 W cm⁻²), reaction for 4 h. a: glucaric acid; b: gluconic acid; c: arabinose; d: glycerol; e: formic acid. (Note: black bar and color bar represent the glucose conversion and product selectivity, respectively.)

3.6. Reasons for enhanced photocatalytic activity

The adsorption of substrate is generally considered to be an important parameter in the photocatalytic process [28]. A comparison of adsorption of glucose on H-ZSM-5 zeolite and H-ZSM-5/FePz(SBu)₈ was performed, as shown in Fig. S5. It could be seen that the adsorption capacity of glucose on H-ZSM-5/FePz(SBu)₈ is a little higher than that of H-ZSM-5 zeolite, the increase of adsorption capacity is beneficial to the improvement of photocatalytic activity. In addition, the transient photocurrent is usually used to assess the charge separation efficiency in the composite photocatalyst [29]. In order to further illustrate the reason for the enhancement of photocatalytic activity of H-ZSM-5/FePz(SBu)₈, the transient photocurrent response versus time curves of the H-ZSM-5/FePz(SBu)₈, pure H-ZSM-5 zeolite and pure FePz(SBu)₈ were measured under irradiation of a LED lamp emitted mainly at 420 nm in an on-and-off cycle mode, as shown in Fig. 10. From Fig. 10, very weak photocurrent was observed in the presence of pure H₂O₂ because of the possible H₂O₂ photolysis induced by visible light. Though very weak photocurrent was also observed in presence of H-ZSM-5 zeolite, the photocurrent value was basically the same as that obtained in the presence of pure H₂O₂, indicating that nearly no photocurrent was generated from the pristine H-ZSM-5 zeolite. However, it can be seen that the H-ZSM-5/FePz(SBu)₈ sample shows a higher photocurrent value than that of pure FePz(SBu)₈, indicating that there exists a synergistic effect between FePz(SBu)₈ and H-ZSM-5 zeolite. The high photocurrent value of composite H-ZSM-5/FePz(SBu)₈ indicates a higher separation efficiency of photon-generated carriers, which is favorable for the photocatalytic activity. Therefore, it turned out that the H-ZSM-5/FePz(SBu)₈ will exhibit a higher photocatalytic activity compared with the pure FePz(SBu)₈, which is good agree with the above results. Therefore, H-ZSM-5 zeolite not only acts as the support, but also provides a synergistic action in the present study.

3.7. Detection of active oxygen species

In order to investigate the mechanism for the photocatalytic oxidation of glucose to value-added chemicals over H-ZSM-5/FePz(SBu)₈. The reactive oxygen species generated from H-ZSM-5/FePz(SBu)₈ in the photocatalytic process were detected by means of ESR technology and scavenger experiments. Fig. 11 shows the ESR signals of active oxygen species generated from H-ZSM-5/FePz(SBu)₈ photocatalytic system. 5,5-dimethyl-1-pyrroline-N-oxide (DMPO) was used as spin trap for capturing superoxide anion

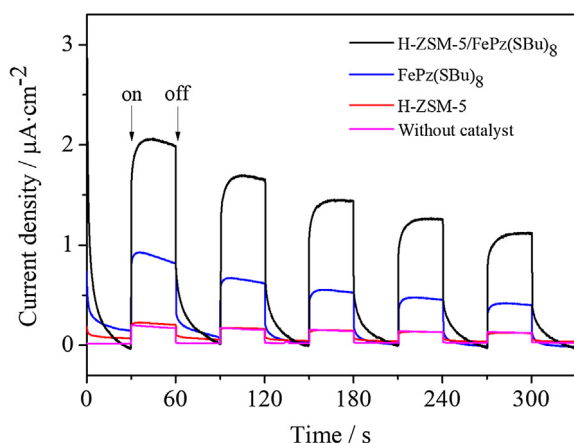


Fig. 10. The transient photocurrent density response of pure H-ZSM-5 zeolite, pure FePz(SBu)₈ and H-ZSM-5/FePz(SBu)₈(5%).

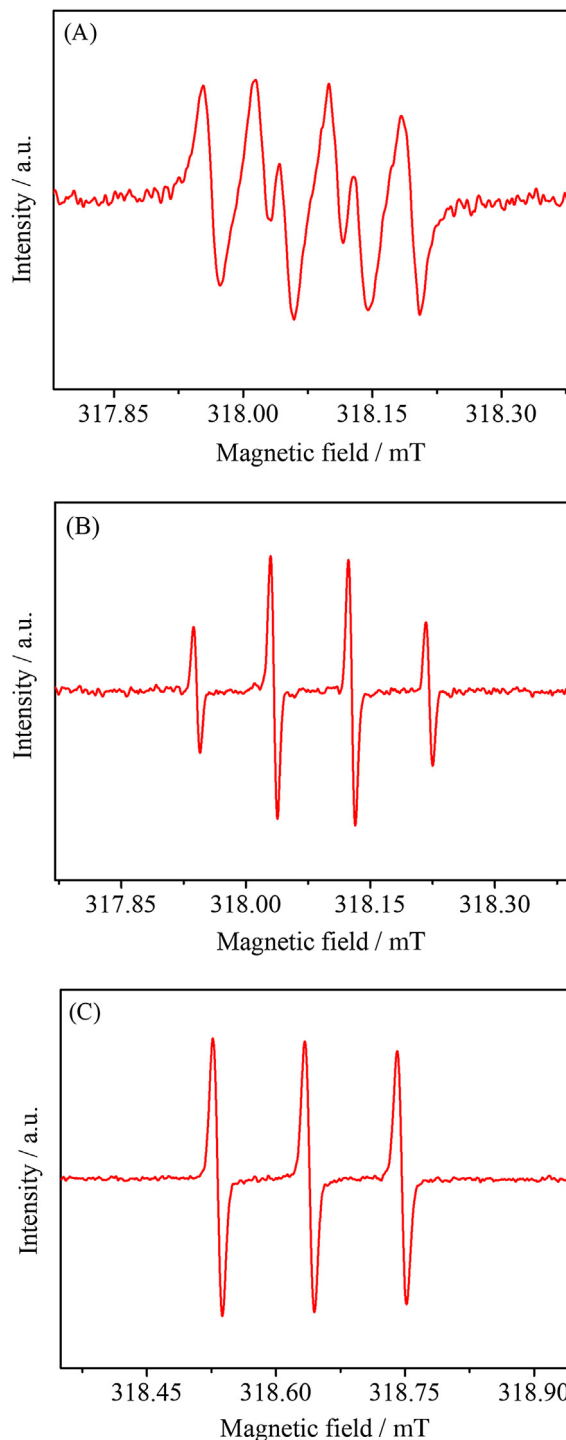
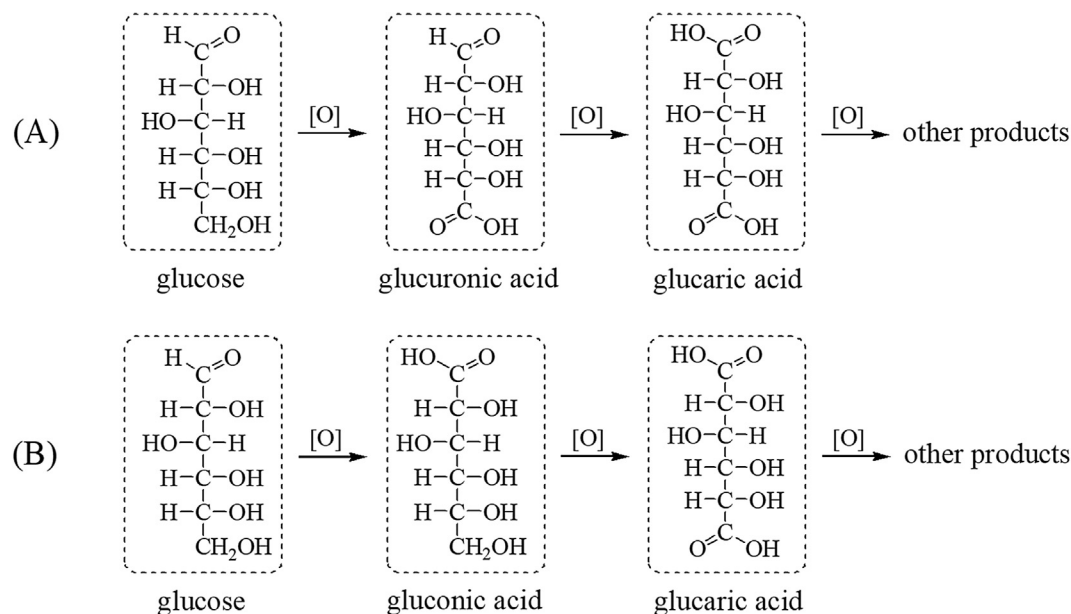


Fig. 11. ESR signals of DMPO- $\text{O}_2^{\cdot-}$ adduct (A), DMPO- $\cdot\text{OH}$ adduct (B) and TEMP- $^1\text{O}_2$ adduct (C) over H-ZSM-5/FePz(SBu)₈(5%) under $\lambda \geq 420$ nm visible light irradiation for 12 min. ESR signals of $^1\text{O}_2$ and $\cdot\text{HO}^{\cdot}$ were detected in aqueous solution, while the ESR signals of $\text{O}_2^{\cdot-}$ were detected in methanol solution.

radical ($\text{O}_2^{\cdot-}$) and hydroxyl radicals ($\cdot\text{OH}$), and 2,2,6,6-tetramethyl piperidine (TEMP) was used to detect the singlet oxygen ($^1\text{O}_2$). According to the characteristic for the spin adduct, it could be seen that strong signals of $\text{O}_2^{\cdot-}$, $\cdot\text{OH}$ and $^1\text{O}_2$ are detected in the presence of H-ZSM-5/FePz(SBu)₈. It was reported that metal complex, such as nickel (II) complex of glycylglycyl-L-histidine, can react with hydrogen peroxide to produce $\text{O}_2^{\cdot-}$, $\cdot\text{OH}$ and $^1\text{O}_2$ [30]. Further, the scavenger experiments were conducted by using various



Scheme 1. The plausible reaction routes for photocatalytic oxidation of aqueous glucose with H-ZSM-5/FePz(SBu)₈.

scavengers, such as 2,2,6,6-tetramethylpiperidine-1-oxyl radical (TEMPO) as O_2^- scavenger, isopropanol (IPA) as $\cdot OH$ scavenger and β -carotene as 1O_2 scavenger. A procedure for scavenger experiments was described in detail in the Supporting Information. As shown in Fig. S6, it could be seen that all three scavengers exhibit inhibitory effect on the photocatalytic oxidation of glucose. The dramatic decline of glucose conversion was observed in the presence of TEMPO and IPA, suggesting that O_2^- and $\cdot OH$ are the main active oxygen species dominated the photocatalytic reaction. The O_2^- and $\cdot OH$ could be stabilized in the pores of H-ZSM-5 zeolite, which consequently benefits the photocatalytic oxidation of glucose. In addition, β -carotene exhibited a moderate inhibitory effect on the photocatalytic process, indicating that 1O_2 is also the active oxygen species in the H-ZSM-5/FePz(SBu)₈ catalytic system. These results are good consistent with the results of ESR.

3.8. Possible reaction pathways

In order to explore the reaction pathways for glucose oxidation, the distribution of products as a function of reaction time was investigated over H-ZSM-5/FePz(SBu)₈ under visible light irradiation. As illustrated in Fig. S7, the glucose conversion increases with the extension of reaction time, which is up to 67% after reaction for 6 h. But no significantly improved glucose conversion is observed after reaction for 8 h, maybe because the oxidant H_2O_2 is almost completely consumed and the glucose conversion is very low in the case of O_2 (Table 1, Entry 7). In the initial stage, five products such as glucaric acid, gluconic acid, arabinose, glycerol and formic acid are obtained, the total selectivity reaches up to 90.3%. For glucaric acid, gluconic acid and arabinose, their selectivity gradually increases firstly and then remarkably gradually decreases with reaction time, and the maximum selectivity is obtained over 4 h. Especially, the total selectivity for glucaric acid and gluconic acid reaches up to 45% over 4 h. While as for glycerol and formic acid, both have the maximum selectivity at the beginning of the reaction, then a remarkable reduction of selectivity is observed in comparison to the initial value although the selectivity don't change when the reaction time exceeds 2 h.

On the basis of the above analysis, five oxidation products containing glucaric acid, gluconic acid, arabinose, glycerol and formic

acid could be obtained from the photocatalytic oxidation of glucose in water. Apart from these five products in the HPLC-MS analysis, glucuronic acid was also detected, as shown in Fig. S8. But it was not detected in the HPLC analysis, maybe owing to its very low content. In order to expound the pathway of oxidation of glucose, a series of experiments using glucuronic acid, glucaric acid and gluconic acid as substrates were further carried out in presence of H-ZSM-5/FePz(SBu)₈(5%) under visible light irradiation. It was found that glucuronic acid could be oxidized to glucaric acid through the HPLC-MS analysis of the oxidation products of glucuronic acid, indicating that glucuronic acid may be an intermediate product for the photocatalytic oxidation of glucose and the formed glucuronic acid could be subsequently transformed into glucaric acid by the reactive oxygen species. Meanwhile, oxidation of glucaric acid could produce arabinose, glycerol and formic acid through the HPLC-MS analysis of the oxidation products. It is noteworthy that oxidation of gluconic acid could also produce glucaric acid (Fig. S9). It suggests that the glucaric acid is produced by two ways, one is the oxidation of glucuronic acid and the other is the oxidation of gluconic acid. Therefore, the possible process pathways (Scheme 1) are as follows: Firstly, the reactive oxygen species generated in the photocatalytic process can attack the C1 and C6 atoms of glucose to produce the gluconic acid and glucuronic acid. Then, a further oxidative attack to the obtained gluconic acid molecule and glucuronic acid molecule releases glucaric acid, and in turn, glucaric acid molecule can be transformed into other products by an oxidative attack, such as arabinose, glycerol and formic acid, and so on.

4. Conclusions

In conclusion, a new complex iron tetra(2,3-bis(butylthio)mal eonitrile)porphyrzine (FePz(SBu)₈) was successfully synthesized. This work further showed that visible light ($\lambda \geq 420$ nm) can be used to transform glucose in water to value-added chemicals such as glucaric acid, gluconic acid, arabinose, glycerol and formic acid in presence of H-ZSM-5/FePz(SBu)₈ photocatalysts using H_2O_2 as oxidant. It is noteworthy that the total selectivity for glucaric acid and gluconic acid reaches up to 45% with moderate conversion of glucose (about 35.8%) after 4 h visible light irradiation, when the

concentration of aqueous glucose is 3 mmol L⁻¹ and H₂O₂:glucose ratio is 3.3:1. The high photocatalytic activity of H-ZSM-5/FePz (SBU)₈ is mainly due to the synergistic effect between FePz(SBU)₈ and H-ZSM-5 zeolite. With the assistance of reactive oxygen species including O₂⁻, ·OH and ¹O₂, the conversion of glucose is accomplished through multiple parallel and subsequent reactions. The present work affords a fine example for conversion of glucose to value-added chemicals in aqueous media under mild conditions using sunlight as light source.

Acknowledgements

This work was supported by the National Natural Science Foundation of China (No. 21772237), Natural Science Foundation of Hubei Province (No. 2018CFB494), “the Fundamental Research Funds for the Central Universities”, South-Central University for Nationalities (No. CZY14003) and the State Foundation for Studying Abroad (201707780019).

Appendix A. Supplementary material

Supplementary data to this article can be found online at <https://doi.org/10.1016/j.jcat.2019.04.044>.

References

- [1] W. Deng, Q. Zhang, Y. Wang, Catalytic transformations of cellulose and cellulose-derived carbohydrates into organic acids, *Catal. Today* 234 (2014) 31–41.
- [2] C. Chatterjee, F. Pong, A. Sen, Chemical conversion pathways for carbohydrates, *Green Chem.* 17 (2015) 40–71.
- [3] A. Corma, S. Iborra, A. Velty, Chemical routes for the transformation of biomass into chemicals, *Chem. Rev.* 107 (2007) 2411–2502.
- [4] M. Besson, P. Gallezot, C. Pinel, Conversion of biomass into chemicals over metal catalysts, *Chem. Rev.* 114 (2014) 1827–1870.
- [5] E. Derrien, M. Mounguengui-Diallo, N. Perret, P. Marion, C. Pinel, M. Besson, Aerobic oxidation of glucose to glucaric acid under alkaline-free conditions: Au-based bimetallic catalysts and the effect of residues in a hemicellulose hydrolysate, *Ind. Eng. Chem. Res.* 56 (2017) 13175–13189.
- [6] N. Dimitratos, J.A. Lopez-Sanchez, G.J. Hutchings, Selective liquid phase oxidation with supported metal nanoparticles, *Chem. Sci.* 3 (2012) 20–44.
- [7] Y.-P. Liu, P. Zheng, Z.-H. Sun, Y. Ni, J.-J. Dong, P. Wei, Strategies of pH control and glucose-fed batch fermentation for production of succinic acid by *Actinobacillus succinogenes* CGMCC1593, *J. Chem. Technol. Biotechnol.* 83 (2008) 722–729.
- [8] M.A. Patel, M.S. Ou, R. Harbrucker, H.C. Aldrich, M.L. Buszko, L.O. Ingram, K.T. Shanmugam, Isolation and characterization of acid-tolerant, thermophilic bacteria for effective fermentation of biomass-derived sugars to lactic acid, *Appl. Environ. Microbiol.* 72 (2006) 3228–3235.
- [9] J. Payormhorm, S. Chuangchote, N. Laosiripojana, CTAB-assisted sol-microwave method for fast synthesis of mesoporous TiO₂ photocatalysts for photocatalytic conversion of glucose to value-added sugars, *Mater. Res. Bull.* 95 (2017) 546–555.
- [10] B. Jin, G. Yao, X. Wang, K. Ding, F. Jin, Photocatalytic oxidation of glucose into formate on nano TiO₂ catalyst, *ACS Sustain. Chem. Eng.* 5 (2017) 6377–6381.
- [11] M. Bellardita, E.I. García-López, G. Marci, B. Megna, F.R. Pomilla, L. Palmisano, Photocatalytic conversion of glucose in aqueous suspensions of heteropolyacid-TiO₂ composites, *RSC Adv.* 5 (2015) 59037–59047.
- [12] J.C. Colmenares, A. Magdziarz, A. Bielejewska, High-value chemicals obtained from selective photo-oxidation of glucose in the presence of nanostructured titanium photocatalysts, *Bioresour. Technol.* 102 (2011) 11254–11257.
- [13] J.C. Colmenares, A. Magdziarz, Room temperature versatile conversion of biomass-derived compounds by means of supported TiO₂ photocatalysts, *J. Mol. Catal. A: Chem.* 366 (2013) 156–162.
- [14] M. Bellardita, E.I. García-López, G. Marci, L. Palmisano, Photocatalytic formation of H₂ and value-added chemicals in aqueous glucose (Pt)-TiO₂ suspension, *Int. J. Hydrogen Energy* 41 (2016) 5934–5947.
- [15] L.D. Vià, C. Recchi, E.O. Gonzalez-Yañez, T.E. Davies, J.A. Lopez-Sanchez, Visible light selective photocatalytic conversion of glucose by TiO₂, *Appl. Catal. B: Environ.* 202 (2017) 281–288.
- [16] L.D. Vià, C. Recchi, T.E. Davies, N. Greeves, J.A. Lopez-Sanchez, Visible-light-controlled oxidation of glucose using titania-supported silver photocatalysts, *ChemCatChem.* 8 (2016) 3475–3483.
- [17] Q. Xiao, E. Jaatinen, H. Zhu, Direct photocatalysis for organic synthesis by using plasmonic-metal nanoparticles irradiated with visible light, *Chem. Asian J.* 9 (2014) 3046–3064.
- [18] Y. Rio, M.S. Rodríguez-Morgade, T. Torres, Modulating the electronic properties of porphyrinoids: a voyage from the violet to the infrared regions of the electromagnetic spectrum, *Org. Biomol. Chem.* 6 (2008) 1877–1894.
- [19] T.V. Dubinina, N.E. Borisova, M.V. Sedova, L.G. Tomilova, T. Furuyama, N. Kobayashi, Synthesis and spectral properties of nonclassical binuclear thienoporphyrazines, *Dyes Pigm.* 117 (2015) 1–6.
- [20] G. Ricciardi, A. Rosa, I. Ciofini, A. Bencini, Synthesis, structure, and physicochemical properties of ((ethylsulfanyl)porphyrinato)cobalt(II). Metal-ligand bonds in Co(OESPz) and in related cobalt(II) tetrapyrroles: insights from a density functional study, *Inorg. Chem.* 38 (1999) 1422–1431.
- [21] H. Li, L. Cao, C. Yang, Z. Zhang, B. Zhang, K. Deng, Selective oxidation of benzyl alcohols to benzoic acid catalyzed by eco-friendly cobalt thioporphyrazine catalyst supported on silica-coated magnetic nanospheres, *J. Environ. Sci.* 60 (2017) 84–90.
- [22] J. Jin, C. Yang, B. Zhang, K. Deng, Selective oxidation of amines using O₂ catalyzed by cobalt thioporphyrazine under visible light, *J. Catal.* 361 (2018) 33–39.
- [23] Q. Zhou, S. Xu, C. Yang, B. Zhang, Z. Li, K. Deng, Modulation of peripheral substituents of cobalt thioporphyrazines and their photocatalytic activity, *Appl. Catal. B: Environ.* 192 (2016) 108–115.
- [24] J. Li, J. Yin, C. Yang, S. Xu, Q. Zhou, B. Zhang, K. Deng, Photocatalyst with annulated binuclear thioporphyrazine-enhancing photocatalytic performance by expansion of a π-electron system, *Catal. Sci. Technol.* 8 (2018) 5616–5622.
- [25] K. Shen, N. Wang, W. Qian, Y. Cui, F. Wei, Atmospheric pressure synthesis of nanosized ZSM-5 with enhanced catalytic performance for methanol to aromatics reaction, *Catal. Sci. Technol.* 4 (2014) 3840–3844.
- [26] S.L. Gojković, S. Gupta, R.F. Savinell, Heat-treated iron(III) tetramethoxyphenyl porphyrin supported on high-area carbon as an electrocatalyst for oxygen reduction, I. characterization of the electrocatalyst, *J. Electrochem. Soc.* 145 (1998) 3493–3499.
- [27] T.-S. Zhao, T. Takemoto, N. Tsubaki, Direct synthesis of propylene and light olefins from dimethylether catalyzed by modified H-ZSM-5, *Catal. Commun.* 7 (2006) 647–650.
- [28] Y. Yu, J.C. Yu, C.-Y. Chan, Y.-K. Che, J.-C. Zhao, L. Ding, W.-K. Ge, P.-K. Wong, Enhancement of adsorption and photocatalytic activity of TiO₂ by using carbon nanotubes for the treatment of azo dye, *Appl. Catal. B: Environ.* 61 (2015) 1–11.
- [29] F. Li, S. Liu, Y. Xue, X. Wang, Y. Hao, J. Zhao, R. Liu, D. Zhao, Structure modification function of g-C₃N₄ for Al₂O₃ in the in situ hydrothermal process for enhanced photocatalytic activity, *Chem. Eur. J.* 21 (2015) 10149–10159.
- [30] S. Inoue, S. Kawanishi, ESR evidence for superoxide, hydroxyl radicals and singlet oxygen produced from hydrogen peroxide and nickel (II) complex of glycylglycyl-L-histidine, *Biochem. Biophys. Res. Commun.* 159 (1989) 445–451.